IJIE

UTHM | Penerbit
Universiti Tun Hussein Onn Malaysia

INTERNATIONAL JOURNAL OF INTEGRATED ENGINEERING
ISSN: 2229-838X e-ISSN: 2600-7916

Vol. 18 No. 3 (2026) 300-310
https://publisher.uthm.edu.my/ojs/index.php/ijie

Single-Camera Guidewire Movement Tracking System in a Concentrically Occluded Configuration for an Endovascular Interventions Simulator Interface

Hazwani Harun[1], Hafiz Rashidi Ramli[1]*, Lenny Suryani Safri[2], M. Iqbal Saripan[3]

[1] *Department of Electric and Electrical Engineering, Faculty of Engineering, Universiti Putra Malaysia, Serdang, MALAYSIA*
[2] *Department of Surgery, Faculty of Medicine, UKM Medical Centre, Cheras, MALAYSIA*
[3] *Department of Computer and Communication Systems Engineering, Faculty of Engineering, Universiti Putra Malaysia, Serdang, MALAYSIA*

*Corresponding Author: hrhr@upm.edu.my
DOI: https://doi.org/10.30880/ijie.2026.18.03.020

Article Info

Received: 8 November 2025
Accepted: 15 April 2026
Available online: 30 April 2026

Keywords

Instruments, testing, catheter, surgery, tracking, robots, biomedical engineering, endovascular devices, instrument testing, modeling

Abstract

Endovascular intervention simulator is a training device for image-guided procedures involving instruments such as guidewires and catheters inserted percutaneously into blood vessels. The efficiency of the simulator relies on the accuracy of its tracking system in estimating the motion of these instruments. Detecting the movement of the guidewire is challenging because it is positioned inside the catheter. To address this, custom markers were developed on the guidewire's surface, and the Gunnar Farneback Algorithm Method was applied to detect its movement. Firstly, a camera records the guidewire's movements. The Gunnar Farneback Algorithm Method then processes the extracted images to obtain raw magnitude and orientation data. This output data was analyzed to get its accuracy and thus validated by comparing experimental values with theoretical values. The results show that the developed tracking system can estimate the distance of the guidewire's movement with an accuracy of 94.43% and 64.80% for the direction. These findings demonstrate that the developed tracking system is effective and sufficient in detecting the movement of a guidewire inside the catheter.

1. Introduction

Endovascular intervention is a minimally invasive alternative for treating vascular diseases such as Abdominal Aortic Aneurysm [1]. This technique involves the navigation of a guidewire and catheter within the blood vessel [2]. The Endovascular Intervention Simulator (EIS), a virtual reality-based training platform, is designed to replicate actual endovascular procedures, thereby enabling surgeons to develop proficiency in these techniques. Studies have demonstrated that EIS facilitates the swift acquisition of technical skills by trainees The simulator's capacity for unlimited practice sessions allows surgeons to refine their skills, which contributes to improved surgical outcomes [4]. Surgeons trained on EIS are able to perform interventions more efficiently, resulting in reduced procedure times and decreased use of contrast agents, thereby enhancing overall success rates [4].

During endovascular intervention simulations, the guidewire is predominantly obscured by the catheter, posing significant challenges in tracking and detecting its movement [5]. This difficulty arises due to the absence of direct contact and the lack of a clear line of sight to the guidewire. This issue, hereafter referred to as the 'Catheter-occluded guidewire' problem, describes the scenario where the catheter concentrically obstructs the guidewire, making it difficult to track and detect, as shown in Fig. 1.

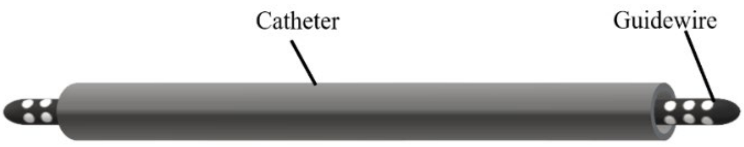

Fig. 1 *Catheter-occluded guidewire inside the catheter*

A reliable tracking system is fundamental to the development of the Endovascular Intervention Simulator (EIS), as it enables precise localization of the guidewire even when obscured by the catheter [5]. High tracking accuracy is critical to ensure that the simulator replicates clinical procedures effectively, thereby achieving strong face validity [6]. The overall performance of the simulator also depends on the capability of its sensing mechanism to capture and process guidewire motion with precision [7].

To address this, the Gunnar Farneback Algorithm Method (GFAM), an optical flow-based approach, is proposed as the core of a custom tracking framework for estimating the movement of the catheter-occluded guidewire. GFAM detects motion by analyzing changes in pixel intensity and displacement between consecutive image frames. Using polynomial expansion, it estimates both translational and rotational motion of the guidewire, generating outputs in terms of magnitude and orientation [8]. The magnitude represents the extent of displacement, whereas the orientation specifies the direction of movement [9]. The accuracy of these measurements directly influences the fidelity and training effectiveness of the EIS [10].

Several optical flow algorithms, including Lucas–Kanade, Horn–Schunck, and DeepFlow, have been widely applied in motion estimation tasks [11], [12], [13]. However, when tracking a guidewire under concentric occlusion, a method that balances computational efficiency with high accuracy is essential. This study evaluates multiple techniques and identifies GFAM as the most suitable choice for this application.

Recent research underscores the versatility of optical flow across diverse domains. In clinical monitoring, for example, group velocity reconstruction methods have been used for seizure and apnea detection, showing resilience to noisy signals and low computational demands [14]. In medical imaging, optical-flow-based techniques have enabled the quantification of diaphragmatic motion from ultrasound scans, facilitating differentiation between healthy individuals and ventilated patients [15]. Beyond medicine, optical flow has been integrated with geometric modeling for real-time contour detection in robotics, illustrating its value in complex, dynamic environments [16]. These advances highlight the robustness of optical flow and support its adoption for guidewire tracking under catheter occlusion.

2. Methodology

The schematic diagram in Fig. 2 presents the experimental setup, comprising the guidewire, catheter, LED, and camera. All components are enclosed within a housing to reduce image noise prior to processing [16]. The guidewire is mounted horizontally and translates along a fixed axis that is perpendicular to the vertically oriented camera. From the camera's perspective, the guidewire appears as a rectangular shape within the field of view. In this arrangement, the guidewire is seen to move laterally left when advancing and right when retracting (Fig. 3(a)). When rotated clockwise or counterclockwise about its axis, it appears to shift vertically within the image frame, corresponding to upward and downward motion, respectively (Fig. 3(b)), with the input slot positioned on the right side.

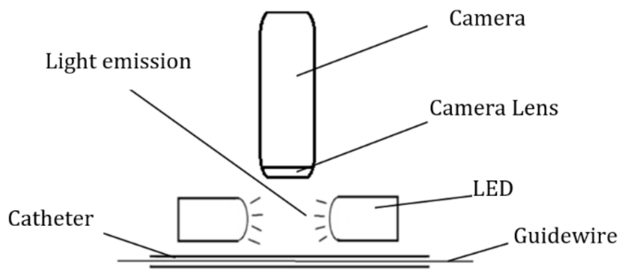

Fig. 2 *Schematic design of configuration setup*

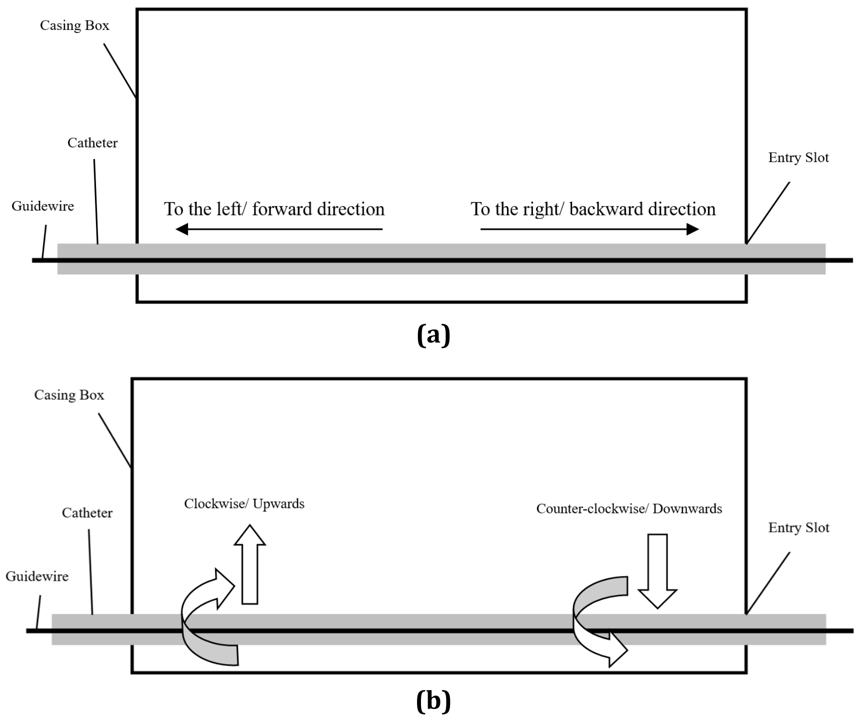

Fig. 3 *Figurative description of the relative the of guidewire's movement; (a) Translational; (b) Rotational*

During video recording for data collection, the guidewire was subjected to both translational and rotational motions, controlled by an automated system [16]. The ground truth dataset was obtained using this motion control system, referred to as the AutoMover Machine, which was programmed to execute predefined translational and rotational movements with high precision. For translational motion, the guidewire was displaced laterally at specified distances (e.g., 3 mm, 6 mm, and 10 mm), while for rotational motion, it was rotated clockwise and counterclockwise at designated angles (e.g., 45°, 90°, and 180°).

Because the AutoMover Machine governed all movements, the programmed values were considered as the ground truth reference for evaluating the tracking system's accuracy. Each motion pattern was repeated several times to ensure reliability and repeatability during validation. The resulting video sequences were captured by the camera and transferred to the processor for image analysis, with the complete set of motion parameters summarized in Table 1.

Table 1 *Sets of movements*

Abbreviation	Movements
3R	3 mm to the right
3L	3 mm to the left
6R	6 mm to the right
6L	6 mm to the left
9R	9 mm to the right
9L	9 mm to the left
10R	10 mm to the right
10L	10 mm to the left
15R	15 mm to the right
15L	15 mm to the left
20R	20 mm to the right
20L	20 mm to the left
45CW	45^0 clockwise
45CCW	45^0 counter-clockwise
90CW	90^0 clockwise

Abbreviation	Movements
90CCW	90^0 counter-clockwise
135CW	135^0 clockwise
135CCW	135^0 counter-clockwise
180CW	180^0 clockwise
180CCW	180^0 counter-clockwise
360CW	360^0 clockwise
360CCW	360^0 counter-clockwise

In addition to adopting GFAM as the primary tracking method, this study also evaluated the Lucas–Kanade and Horn–Schunck algorithms for comparative analysis. All three approaches were tested under identical experimental conditions, and their performances were assessed in terms of both magnitude and orientation accuracy. A detailed comparison of these results is provided in the Results section.

For image processing, GFAM estimates guidewire motion by calculating pixel displacement between successive frames [16]. To enhance motion detection, custom markers were applied to the guidewire surface, as illustrated in Fig. 4. These markers were painted white to maximize light reflection and visibility. They were manually applied and evenly distributed along the guidewire to enable consistent and comprehensive tracking throughout the experiment.

Fig. 4 *Guidewire with white markers on the surface*

Designing a tracking system capable of monitoring guidewire motion is particularly challenging due to the absence of direct visual and tactile feedback, a limitation commonly referred to as the concentric occlusion guidewire problem (Fig. 1). To address this, the present study utilizes a green transparent catheter (Fig. 5). The catheter, made from a soft, hollow polypropylene copolymer, is commonly used in endovascular procedures. Its transparency allows optical sensors to detect the guidewire's motion through the catheter wall. The catheter used in this work measures approximately 0.89 cm in diameter and 300 cm in length.

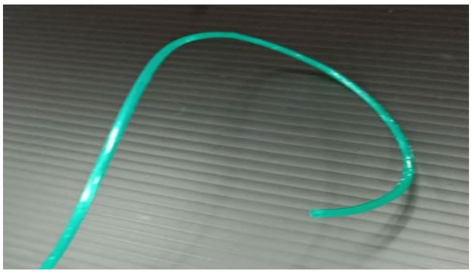

Fig. 5 *The green transparent catheter*

2.1 Gunnar Farneback Algorithm Method

As described earlier, GFAM is an optical flow technique used to estimate guidewire motion by tracking pixel displacement between consecutive image frames [17]. The method applies a polynomial expansion to the intensity variations of two successive frames, leading to the formulation of equations (1) and (2). These equations are then used to compute the pixel displacement vector, as shown in equation (3) [17]. Equation (1) represents the polynomial approximation for frame *n*, while equation (2) corresponds to the subsequent frame *n + 1*. The displacement vector A in equation (3) is resolved into its horizontal (Vx) and vertical (Vy) components, indicating pixel displacements along the *x*- and *y*-axes, respectively. These components form the basis for calculating the motion's orientation and magnitude, as defined in equations (4) and (5) [17].

$$f_1(x) = x^T A_1 x + b_1^T x + c_1 \quad (1)$$

$$
\begin{aligned}
{}_{2} &= f_1(\mathrm{x}\ \ \mathrm{d})^T \mathrm{A1}(\mathrm{x}\ \ \mathrm{d}) + \mathrm{b}_1{}^T(\mathrm{x}\ \ \mathrm{d}) + c_1 \\
&= \mathrm{x}^T\mathrm{A}_1\mathrm{x} + (\mathrm{b}_1\ \ 2\mathrm{A}_1\mathrm{d})^T\mathrm{x} + \mathrm{d}^T\mathrm{A}_1\mathrm{d} + \mathrm{b}_1{}^T\mathrm{d} + c_1 \\
&= \mathrm{x}^T\mathrm{A}_1\mathrm{x} + \mathrm{b}_2{}^T\mathrm{x} + c_2
\end{aligned} \tag{2}
$$

$$\mathrm{A(x)} = \frac{\mathrm{A}_1(\mathrm{x}) + \mathrm{A}_2(\mathrm{x})}{2} \tag{3}$$

$$\text{Orientation} = \mathrm{atan2}(\mathrm{V_y}, \mathrm{V_x}) \tag{4}$$

$$\text{Magnitude} = \sqrt{(\mathrm{V_x.V_x} + \mathrm{V_y.V_y})} \tag{5}$$

In equations (1)–(5), $x = [x\ y]^T$ represents the spatial image coordinates, and $d = [dx\ dy]^T$ denotes the inter-frame displacement vector. A_1 and A_2 are the symmetric coefficient matrices of the quadratic polynomial expansions for two consecutive frames, associated with the first-order vectors b_1, b_2 and constants c_1, c_2. The combined coefficient matrix is expressed as A(x). The optical flow vector is defined as $v = [Vx\ Vy]^T$, where Vx and Vy correspond to horizontal and vertical displacements in pixels per frame, respectively. The flow orientation is computed as atan2(Vy, Vx), while the magnitude is given by $\sqrt{(Vx^2 + Vy^2)}$. Pixel magnitudes are then converted to millimeters using a pre-determined calibration factor.

2.2 Determining Motion of the Guidewire

Fig. 6 shows the flowchart for estimating the guidewire's motion in terms of both direction and distance. After processing with GFAM, two outputs are generated: magnitude, which represents how far the guidewire has moved, and orientation, which indicates the direction of that movement. These outputs are initially produced as images and require additional processing to obtain precise numerical values.

An important point is that orientation depends on magnitude, any change in magnitude directly affects orientation. The magnitude data, however, is independent and can be processed on its own.

For translational movement, the raw magnitude data is first smoothed using a Gaussian Filter with a value of 2 to reduce noise. The movement's direction is then derived from the orientation data using a windowing (segmentation) process with a value of 44. Because orientation relies on magnitude, filtering the magnitude also improves the orientation output before segmentation.

For rotational (angular) movement, the magnitude data goes through two stages of filtering. First, during GFAM processing, a Gaussian Filter with a value of 2 is applied. After the raw data is extracted, it is filtered again with a Gaussian Filter set to 8 to enhance the accuracy of angular displacement. The direction of rotation is then obtained by applying a windowing process with a value of 38 to the orientation data.

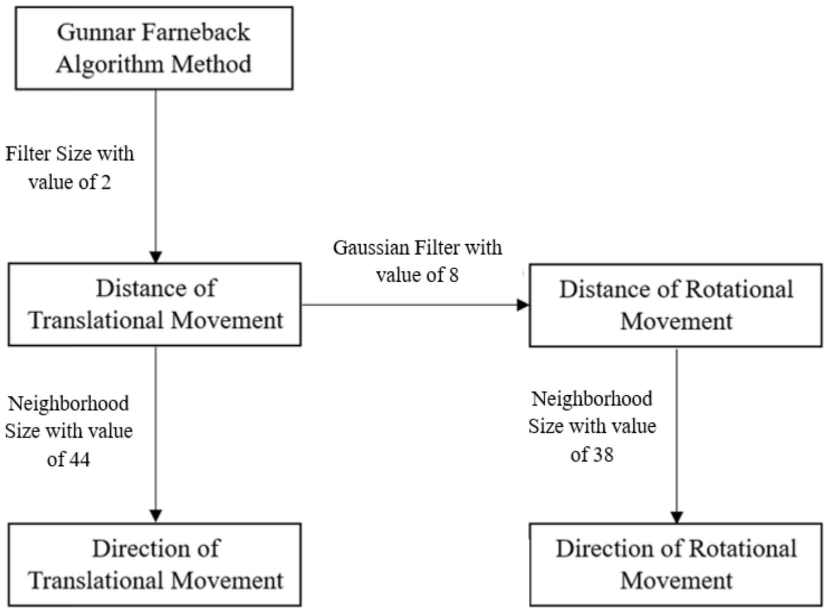

Fig. 6 *Flowchart of motion estimating*

Table 2 *The parameters of gunnar farneback algorithm method*

Parameters	Default Values
Level of Pyramid	3
Pyramid Scale	0.5
Number of Iterations	3
Neighborhood Size	5
Filter Size	15

Table 2 summarizes the parameters used for GFAM. During image processing, the pyramid level, pyramid scale, and number of iterations are kept at minimal values. The pyramid level is particularly important for handling large images by down-sampling them when there is significant pixel displacement, such as in long-distance imaging [18]. In this study, the region of interest (ROI) is relatively small (640 × 110 pixels) with only minimal pixel displacement. Because of this, the pyramid level is set to 1, meaning that only the original image is processed without any decomposition. This ensures the highest resolution is retained [18].

With the pyramid level fixed at 1, the pyramid scale is set to 0.5. Although this value typically controls the down-sampling rate at each pyramid level, its impact here is negligible because only a single level is used [18]. The number of iterations is set to 1 as well, since the small image size does not require additional iterations to reduce computational load. To benchmark GFAM's performance, three optical flow algorithms which is GFAM, Lucas-Kanade, and Horn-Schunck were implemented and tested for their ability to detect guidewire movements.

The parameter choices shown in Table 2 were based on preliminary testing during system development. The low image resolution (640 × 110 pixels) and limited guidewire displacement (~3–20 mm) allowed the use of a single pyramid level and pyramid scale of 0.5 without losing motion sensitivity. A neighborhood size of 5 pixels and one iteration provided sub-pixel accuracy while keeping computation times low. Increasing the neighborhood size or iterations beyond these settings improved accuracy by less than 2% but substantially increased runtime. Thus, the selected parameters provide an effective balance between accuracy and efficiency, enabling near-real-time tracking in the simulator.

3. Results and Discussion

Fig. 7 shows the tracking accuracy for both magnitude and orientation data across all movements. For translational movement, the magnitude data achieves an accuracy between 81.3% and 99.9%. The highest accuracy (99.9%) is recorded during the 15L movement, while the lowest (81.3%) is observed in the 3L movement. For orientation data, the accuracy varies more widely, ranging from 22.2% to 80.6%. The lowest accuracy (22.2%) occurs during the 5L movement, whereas the highest (80.6%) is achieved in the 5R movement

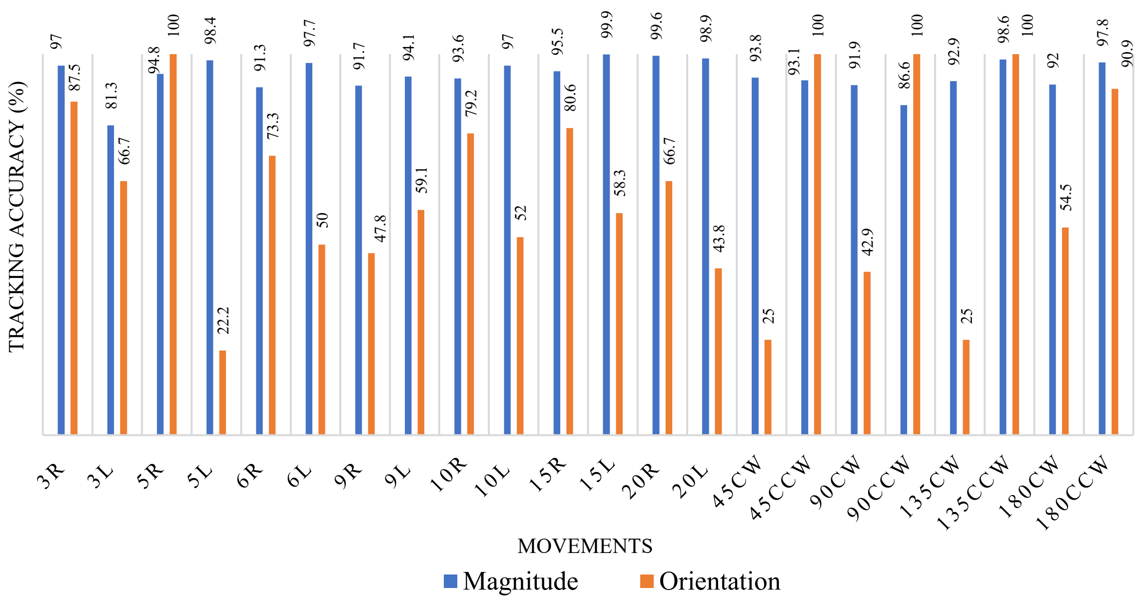

Fig. 7 *Tracking accuracy for magnitude and orientation across all movements; bars show the mean accuracy and error bars denote ±1 SD over three runs (n = 3)*

Int. Journal of Integrated Engineering Vol. 18 No. 3 (2026) p. 300-310

For rotational movement, the magnitude data accuracy ranges from 86.6% to 98.6%. The highest accuracy of 98.6% is observed during the 135CCW movement, while the lowest accuracy of 86.6% occurs during the 90CCW movement. The orientation data accuracy ranges from 25% to 100%, with the lowest accuracy of 25% for 45CW and 135CW movements and the highest accuracy of 100% for 45CCW, 90CCW, and 135CCW movements.

The graph patterns indicate that tracking accuracy is not directly proportional to the guidewire's movement. For instance, movements 5L and 20L have similar accuracies of 98.4% and 98.9%, respectively, despite a 15 mm distance difference. Conversely, a 3 mm movement in the opposite direction (3L) has a lower accuracy of 81.3% compared to the 97.3% accuracy of the 3R movement. On average, the developed tracking system achieves an accuracy of 94.43% ± 1.28% for detecting the guidewire's distance and 64.80% ± 4.15% for detecting its direction (n = 3). The corresponding 95% confidence intervals (computed as in Methods) are indicated by the error bars in Fig. 7. The inclusion of the standard deviation values shows the consistency of tracking the translational movement and highlights the higher variability in orientation movements. Magnitude data consistently shows higher accuracy compared to orientation data, indicating that the system is more proficient at detecting distance than direction.

The results indicate that the system performs better in estimating distance than direction. This difference stems from the use of maximum values for magnitude detection and mode values for orientation detection, as explained earlier. The use of mode data for orientation was necessary to prevent the system from incorrectly interpreting all movements as either leftward or rightward.

As shown in Fig. 7, the orientation data is derived from the most frequent pixel displacement within the image. While this approach should, in theory, provide accurate results, its effectiveness was limited by the irregular shapes of the hand-painted markers. These irregularities reduced the consistency of directional information during optical flow estimation, making orientation tracking less reliable. This limitation highlights the need for improved marker design. Future work could explore markers with asymmetric or direction-specific patterns, as well as printed or laser-etched markers, which would provide more uniform directional cues. Additionally, incorporating preprocessing steps such as contrast enhancement, edge-based segmentation, or adaptive thresholding could further improve orientation accuracy.

In addition to GFAM, two other optical flow methods such as Lucas-Kanade (LK) and Horn-Schunck (HS) were tested for comparison. The results, summarized in Fig. 8, show that GFAM consistently outperformed both methods. GFAM achieved up to 100% orientation accuracy and 95.60% magnitude accuracy, while LK reached 26% for orientation and 90.10% for magnitude, and HS achieved 26% for orientation and 93.72% for magnitude. These results confirm that GFAM offers the best balance of accuracy and computational efficiency for this application. DeepFlow was excluded from the comparison because its high computational cost made it unsuitable for real-time use in the current simulator setup.

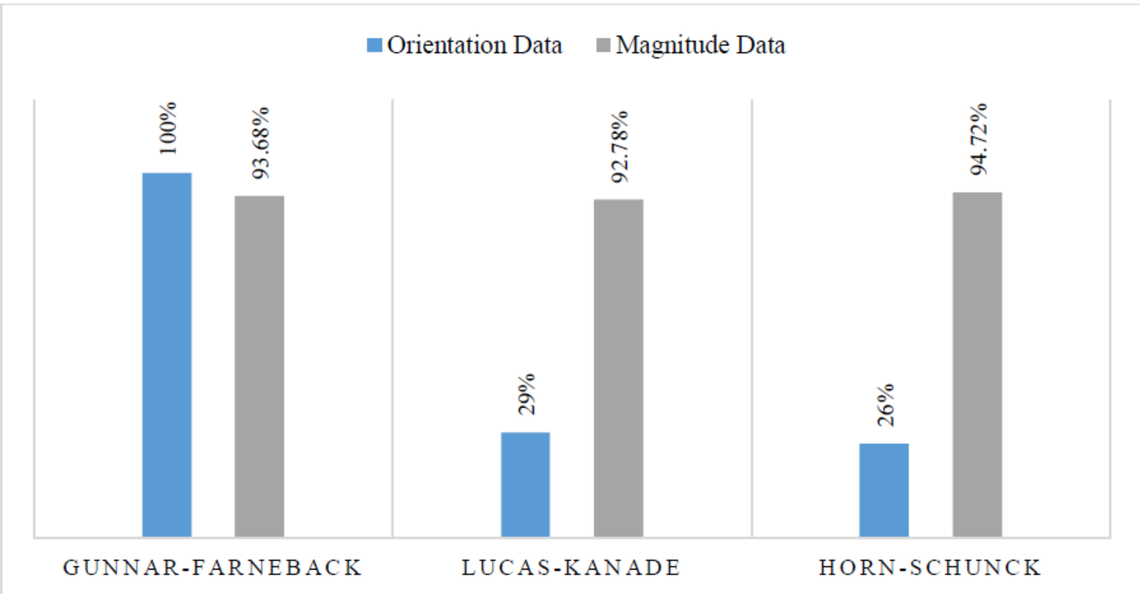

Fig. 8 *Comparison of orientation and magnitude tracking accuracy using three optical flow methods: Gunnar Farneback, Lucas-Kanade, and Horn-Schunck*

To evaluate the consistency of the tracking system, each translational and rotational movement was performed three times. For each movement type, the mean accuracy and standard deviation were calculated, as summarized in Table 3. Confidence intervals were then computed using the formula: Mean ± $t_{0.975,\, df=2} \cdot \frac{SD}{\sqrt{3}}$, where t=4.303 for df=2, with n=3 runs conducted per movement.

Table 3 *Mean accuracy and standard deviation for movement tracking*

Movement Type	Mean Accuracy (%)	Standard Deviation (%)
Translational	94.43	1.28
Rotational	64.80	4.15

The low variability observed in translational accuracy indicates that the system performs consistently when detecting distance-based movements. In contrast, the greater variation in rotational tracking highlights limitations in the current approach to estimating direction, suggesting that further improvements in orientation detection are needed.

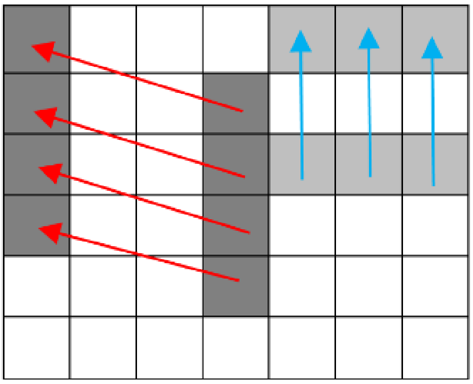

Fig. 9 *The illustration the mode data during pixel displacement*

Fig. 9 illustrates why the tracking system performs well in detecting distance but faces challenges in detecting direction. Distance estimation uses maximum data values, which capture the strongest displacement and ensure accurate results. In contrast, direction estimation relies on mode data values, selecting the most frequent displacement direction among pixels. As shown in the figure, blue arrows represent the correct direction, while red arrows indicate incorrect ones. If the majority of detected displacements are incorrect (red arrows), the mode-based approach will mistakenly select them as the final direction. Fig. 10 shows the actual arrow positions during image processing, captured prior to data filtering and further refinement, highlighting the noisy nature of the raw orientation data.

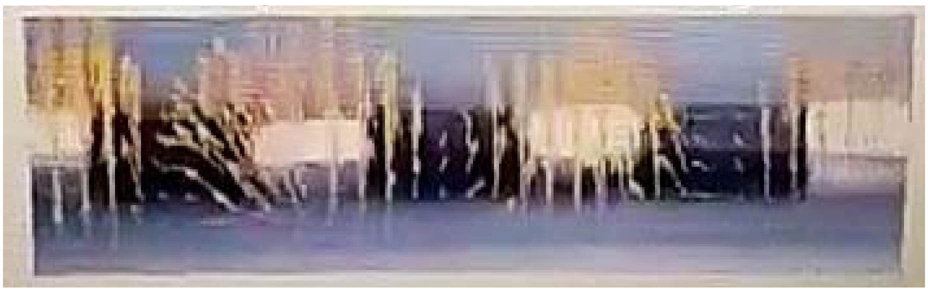

Fig. 10 *The vectors generated by the optical flow algorithm*

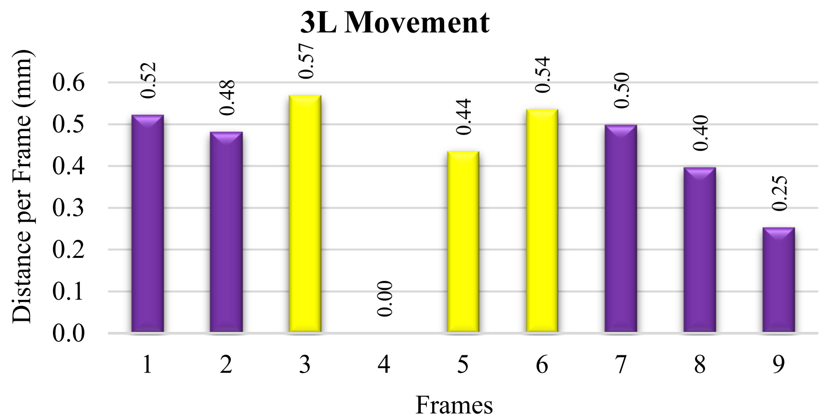

(a)

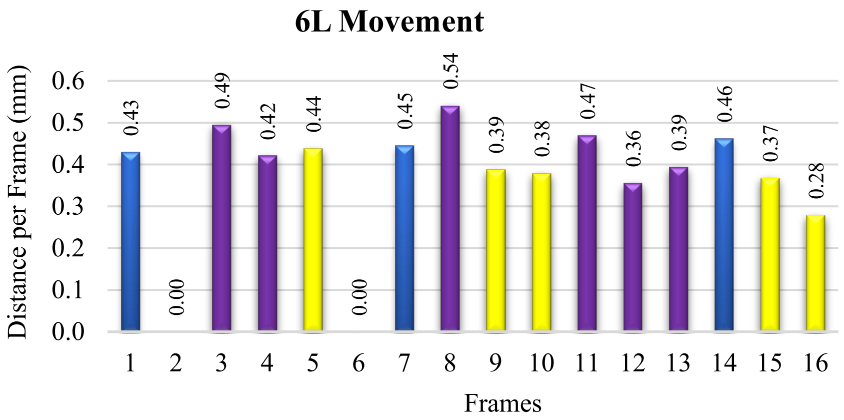

(b)

Fig. 11 *Tracking accuracy results during (a) 3L; and (b) 6L movements*

Fig. 11 shows the tracking accuracy results for movements 3L and 6L. Both movements had frames with zero displacement values, indicating no measurable movement at those points. For 3L, no displacement was recorded in the fourth frame, even though markers were detected in all frames during preprocessing. This happened because the pixel displacement in that frame was below the high-pass filter threshold of 0.25 mm, so it was excluded from the recorded data. The same issue occurred in the second and sixth frames of the 6L movement.

The GFAM settings from Table 2 were used: pyramid level = 1, pyramid scale = 0.5, iterations = 3, neighborhood size = 5, and filter size = 15. With these settings, translational tracking accuracy reached 94.43%, while orientation accuracy was lower at 64.80%. The lower orientation accuracy is likely due to the hand-painted markers, which lacked clear directional features for optical flow estimation.

This level of orientation accuracy may still be acceptable for early-stage endovascular training, where exact angular control is not critical. For more advanced simulations, improvements are needed. Markers with asymmetrical or directional patterns (such as arrows or fiducial shapes) could provide clearer cues. Using printed or laser-made markers would also ensure more consistent patterns. On the image-processing side, adding methods like contrast enhancement, better segmentation, or learning-based direction estimation could help make orientation tracking more reliable in future versions.

4. Conclusions

Estimating the motion of a guidewire inside a catheter is challenging because visibility is lost and there is no tactile feedback. To address this, a tracking system was developed using image processing techniques, specifically the Gunnar Farneback Algorithm Method (GFAM). Markers were applied to the surface of the guidewire to improve tracking performance. GFAM works by using polynomial expansion equations to calculate pixel movements in consecutive frames, producing magnitude and orientation data. The magnitude data is used to estimate the distance of guidewire movement, while the orientation data is used to estimate its direction.

The results show that the tracking system performs well in estimating guidewire movement. The magnitude data achieved high accuracy for distance measurement, whereas the orientation data could determine the movement direction but with lower accuracy. This difference is mainly due to the irregular shape of the guidewire and the manually applied markers, which sometimes reduced the consistency of directional cues during optical flow estimation.

Although this limitation exists, the findings suggest that the system can still provide reliable motion estimation for early-stage endovascular training. Future improvements could involve refining the marker design with asymmetric or direction-specific patterns and using printed or manufactured markers instead of hand-painted ones. These changes could enhance the accuracy of orientation tracking. Overall, the developed system demonstrates its capability to estimate the motion of a catheter-occluded guidewire effectively within the context of endovascular intervention

Acknowledgement

The authors acknowledged the financial support from the Ministry of Higher Education Malaysia through Prototype Research Grant Scheme (PRGS) PRGS/1/2017/TK04/UPM/01/3.

Conflict of Interest

Authors declare that there is no conflict of interests regarding the publication of the paper.

Author Contribution

The authors confirm contribution to the paper as follows: ***study conception and design:*** *Hazwani Harun, Hafiz Rashidi Ramli, M. Iqbal Saripan, Lenny Suryani Safri;* ***data collection:*** *Hazwani Harun;* ***analysis and interpretation of results:*** *Hazwani Harun, Hafiz Rashidi Ramli;* ***draft manuscript preparation:*** *Hazwani Harun, Hafiz Rashidi Ramli. All authors reviewed the results and approved the final version of the manuscript.*

References

[1] F. J. Joseph, H. E. R. Vanluchene, and D. Bervini, “Simulation training approaches in intracranial aneurysm surgery—a systematic review,” *Neurosurg. Rev.*, vol. 46, no. 1, p. 101, May 2023, doi: 10.1007/s10143-023-01995-5.

[2] Y. Cho, J.-H. Park, J. Choi, and D. E. Chang, “Image Processing Based Autonomous Guidewire Navigation in Percutaneous Coronary Intervention,” in *2021 IEEE International Conference on Consumer Electronics-Asia (ICCE-Asia)*, IEEE, Nov. 2021, pp. 1–6. doi: 10.1109/ICCE-Asia53811.2021.9641975.

[3] A. Ramjeeawon, A. E. Sharrock, A. Morbi, G. Martin, C. Riga, and C. Bicknell, “Using Fully-Immersive Simulation Training with Structured Debrief to Improve Nontechnical Skills in Emergency Endovascular Surgery.,” *J. Surg. Educ.*, vol. 77, no. 5, pp. 1300–1311, 2020, doi: 10.1016/j.jsurg.2020.03.023.

[4] A. Haiser, A. Aydin, B. Kunduzi, K. Ahmed, and P. Dasgupta, “A Systematic Review of Simulation-Based Training in Vascular Surgery,” *J. Surg. Res.*, vol. 279, pp. 409–419, Nov. 2022, doi: 10.1016/j.jss.2022.05.009.

[5] H. R. Ramli, N. Misron, M. I. Saripan, and F. Bello, “Development of a Haptic Feedback Actuator for an Endovascular Interventions Simulator Interface,” in *2019 IEEE International Symposium on Haptic, Audio and Visual Environments and Games (HAVE)*, IEEE, Oct. 2019, pp. 1–6. doi: 10.1109/HAVE.2019.8921157.

[6] M. Hong, J. W. Rozenblit, and A. J. Hamilton, “Simulation-based surgical training systems in laparoscopic surgery: a current review,” *Virtual Real.*, vol. 25, no. 2, pp. 491–510, Jun. 2021, doi: 10.1007/s10055-020-00469-z.

[7] J. Guo, M. Li, Y. Wang, and S. Guo, “An Image Information-Based Objective Assessment Method of Technical Manipulation Skills for Intravascular Interventions.,” *Sensors (Basel).*, vol. 23, no. 8, Apr. 2023, doi: 10.3390/s23084031.

[8] D. A. Gutiérrez-Jiménez, S. Salazar-Colores, F. F. Rivera, and J. T. López-Maldonado, “A Novel Method Based on Gunnar Farneback Method, Mathematical Morphology, and Artificial Vision for Flow Analysis in Electrochemical Reactors,” 2023, pp. 133–156. doi: 10.1007/978-3-031-45316-8_11.

[9] M. Almatrafi, R. Baldwin, K. Aizawa, and K. Hirakawa, “Distance Surface for Event-Based Optical Flow,” *IEEE Trans. Pattern Anal. Mach. Intell.*, vol. 42, no. 7, pp. 1547–1556, Jul. 2020, doi: 10.1109/TPAMI.2020.2986748.

[10] W. Duan *et al.*, “Technical and Clinical Progress on Robot-Assisted Endovascular Interventions: A Review,” *Micromachines*, vol. 14, no. 1, p. 197, Jan. 2023, doi: 10.3390/mi14010197.

[11] S. Al-Qudah and M. Yang, "Large Displacement Detection Using Improved Lucas–Kanade Optical Flow," *Sensors*, vol. 23, no. 6, p. 3152, Mar. 2023, doi: 10.3390/s23063152.

[12] A. Elasri, L. Cherroun, and M. Nadour, "Robotic Visual-Based Navigation Structures Using Lucas-Kanade and Horn-Schunck Algorithms of Optical Flow," *Iran. J. Sci. Technol. Trans. Electr. Eng.*, vol. 48, no. 3, pp. 1149–1172, Sep. 2024, doi: 10.1007/s40998-024-00722-0.

[13] T. Calò and L. De Russis, "DeepFlow: A Flow-Based Visual Programming Tool for Deep Learning Development," in *Proceedings of the 30th International Conference on Intelligent User Interfaces*, New York, NY, USA: ACM, Mar. 2025, pp. 504–518. doi: 10.1145/3708359.3712109.

[14] S. Karpuzov, G. Petkov, S. Ilieva, A. Petkov, and S. Kalitzin, "Object Tracking Based on Optical Flow Reconstruction of Motion-Group Parameters," *Information*, vol. 15, no. 6, p. 296, May 2024, doi: 10.3390/info15060296.

[15] Q. Zhang, D. Yang, Y. Zhu, Y. Liu, and X. Ye, "An optimized optical-flow-based method for quantitative tracking of ultrasound-guided right diaphragm deformation," *BMC Med. Imaging*, vol. 23, no. 1, p. 108, Aug. 2023, doi: 10.1186/s12880-023-01066-7.

[16] A. Abu-Jassar, V. Yevsieiev, and S. Maksymova, "The Optical Flow Method and Graham's Algorithm Implementation Features for Searching for the Object Contour in the Mobile Robot's Workspace," vol. 2, no. 3, pp. 306–312, 2024.

[17] O. V. Panchenko and I. A. Ramazanov, "Investigation of the Method of Interpolation of Movement to Video Frames," in *2021 International Russian Automation Conference (RusAutoCon)*, IEEE, Sep. 2021, pp. 745–750. doi: 10.1109/RusAutoCon52004.2021.9537314.

[18] T. Kelemenová, O. Benedik, and I. Koláriková, "SIGNAL NOISE REDUCTION AND FILTERING," *Acta Mechatronica*, vol. 5, no. 2, pp. 29–34, Jun. 2020, doi: 10.22306/am.v5i2.65.